

# **Cine Phase-Contrast Magnetic Resonance Imaging Of Cerebrospinal Fluid Flow**

## **Thesis**

Submitted For Partial Fulfillment Of The Requirements Of The  
MD Degree In Diagnostic Radiology

**By**

**Nermeen Mohammed Abd-Elwahab Hammouda**  
(MBBCH, MSC)  
Radiologist

## **Supervisors**

**Dr. Rashad Hassan Hamdy**

Professor of Diagnostic Radiology  
Faculty of Medicine / Cairo University

**Dr. Ahmed Zohdi Mustafa Zohdi**

Professor of Neurosurgery  
Faculty of Medicine / Cairo University

**Dr. Rami Edward Asaad**

Lecturer of Diagnostic Radiology  
Faculty of Medicine / Cairo University

Diagnostic Radiology Department  
Faculty of Medicine/Cairo University  
2009

بِسْمِ اللَّهِ الرَّحْمَنِ الرَّحِيمِ

فَأَمَّا الزَّبَدُ فَيَذْهَبُ جُفَاءً وَأَمَّا مَا يَنْفَعُ النَّاسَ فَيَمْكُثُ  
فِي الْأَرْضِ كَذَلِكَ يَضْرِبُ اللَّهُ الْأَمْثَالَ

سورة الرعد الآية 17

---

# Acknowledgments

I want to express my gratitude to Dr. Rashad Hassan Hamdy, professor of diagnostic radiology, Cairo university, who originally proposed that I work on this thesis and whose continuous guidance encouraged me to finish it properly.

I also want to acknowledge the crucial role of Dr. Ahmed Zohdi Mustafa Zohdi, Professor of neurosurgery, Cairo university, whose valuable ideas enriched this work.

Also I would like to thank Dr. Rami Edward Asaad, Lecturer of diagnostic radiology, Cairo university, for his continuous help and sincere support.

And I need to express my gratitude to Dr. Yaser abdel-Azim, Professor of diagnostic radiology, Ain-Shams university, for his kind assistance and for the valuable materials he brought us.

I also want to thank the distinguished operators of the MRI unit of Kasr El-Ainy diagnostic radiology department: Miss Amal Mahmoud, Miss Azza Hafez, Miss Hala Ali, Miss Hanan Abdel-Fatah, for their honest and sincere performance. Thanks extend to the nursing staff of the MRI unit.

This work could not have been accomplished had I not had the help and support of my beloved family who brought me so much love and sympathy during last four years.

Nermeen M. abdel-Wahab

2009

---

# **Abstract**

باللغة العربية :

الكلمات الدالة: الرنين المغناطيسي - الاستسقاء المخي - عيوب كيارى 1 الخلقية

تهدف الدراسة المقدمة إلى دراسة ديناميكية تدفق السائل المخي الشوكي في قناة سيلفيس و التجايف تحت العنكبوتية العنقية في الأشخاص الأصحاء و في مرضى الاستسقاء المخي المتصل و الضمور المخي و ضيق قناة سيلفيس و عيوب كيارى 1 الخلقية و ذلك باستخدام الرنين المغناطيسي ذي التباين الوضعي

## **Abstract**

**Keywords: Hydrocephalus – Phase-contrast MRI – Chiari 1 malformation.**

**Cardiac-gated cine Phase contrast MRI has proved to be a robust technique for noninvasive assessment of the hydrodynamics of the CSF circulation. The technique permits both qualitative and quantitative evaluation of CSF flow.**

## List of abbreviations

CSF	Cerebrospinal Fluid
2-D	Two-dimensional
DSV	Diastolic Stroke Volume
ECG	Electrocardiogram
FOV	Field-Of-View
AHS	Adult Hydrocephalus Syndrome
IAHS	Idiopathic Adult Hydrocephalus Syndrome
SD	Standard Deviation
SV	Stroke Volume
SSV	Systolic Stroke Volume
MR	Magnetic Resonance
MRI	Magnetic Resonance Imaging
NPH	Normal-Pressure Hydrocephalus
PC	Phase-Contrast
PDF	Peak Diastolic Flow Rate
PDV	Peak Diastolic Velocity
PSV	Peak Systolic Velocity
ROI	Region-Of-Interest
PET	Positron Emission Tomography
R-PSV	R-Wave To Peak Systolic Velocity
PPU	Finger Pulsimeter
R-S	R-Wave To Onset Of CSF Systole
PSF	Peak Systolic Flow Rate

# **Contents**

Introduction.....	1
Anatomy Of The Ventricular System With MR Imaging Correlation.....	2
Anatomy Of The Subarachnoid Space.....	12
Cerebrospinal Fluid.....	16
Hydrocephalus: Classification And Etiology.....	18
Chiari 1 Malformations.....	32
MR Imaging Of Hydrocephalus.....	36
2-D Cine-Phase-Contrast MRI Of CSF Flow.....	46
Materials And Methods.....	71
Results.....	74
Case Presentation.....	99
Discussion.....	159
Conclusions.....	168
References.....	169
Arabic Summary.....	178

# **List Of Figures**

Figure 1.1. Resin cast of the ventricular system.

Figure 1.2-1.10 Diagrams and MRI images of normal brain.

Figure 2.1. Diagram of the principal subarachnoid cisterns.

Figure 2.2. Relationship of pia and arachnoid to the dura, brain and vessels.

Figure 2.3. Arachnoid villi and granulations.

Figure 3.1. Sagittal T1-W MRI images of cervical spine in Chiari 1 patient.

Figure 3.2. Illustration of normal CSF flow at foramen magnum.

Figure 4.1. MRI of leptomeningeal enhancement (obstructive hydrocephalus).

Figure 4.2. MRI periventricular edema (obstructive hydrocephalus).

Figure 4.3. Normal midsagittal morphology of the brain.

Figure 4.4. MRI of midsagittal changes in obstructive hydrocephalus.

Figure 4.5. MRI Benign external hydrocephalus.

Figure 4.6. MRI of aqueductal stenosis.

Figure 4.7. CSF spaces in IAHS.

Figure 4.8. MRI of IAHS.

Figure 4.9. Grades of flow voids in IAHS.

Figure 5.1. Illustration of phase shifts in moving and nonmoving spins.

Figure 5.2. Illustration of the principle of phase-contrast MRI technique.

Figure 5.3. Normal CSF flow phase-contrast images in sagittal plane.

Figure 5.4. Partial volume effects of CSF flowmetry in the sagittal plane.

Figure 5.5. Phase-contrast images of subarachnoid space at C2 level.

Figure 5.6. Position of the localizer for aqueduct imaging (inferior colliculus).

Figure 5.7. Different positions of the localizers for imaging of the aqueduct.

Figure 5.8. Graph of CSF flow waveform.

Figure 5.9. Temporal analysis of CSF flow velocity images.

Figure 5.10. Functional analysis of CSF flow waveform.

Figure 5.11. Aqueductal CSF flow study in IAHS.

# **List Of Figures**

Figure 5.12. Aqueductal CSF flow study in IAHS

Figure 5.13. Normal phase-contrast images of the foramen magnum.

Figure 5.14. Phase-contrast images of the foramen magnum in Chiari 1.

Figure 5.15. Phase-contrast images of syringomelia

Figure 5.16. Pre- and postoperative evaluation of syringomyelia

Figure 6.1. Boxplot illustrations of the aqueductal CSF flow parameters.

Figure 6.2: Boxplot illustration of PSV in the normal control and Chiari 1 patients

Figure 7.1 –7.7. Case 1

Figure 7.8 – 7.10. Case 2

Figure 7.11 – 7.17. Case 3

Figure 7.18 – 7.22. Case 4

Figure 7.23 – 7.25. Case 5

Figure 7.26 – 7.27. Case 6

Figure 7.28 – 2.29. Case 7

Figure 7.30 – 7.32. Case 8

Figure 7.33 – 7.34. Case 9

Figure 7.35 – 7.49. Case 10

Figure 7.50 – 7.57. Case 11

Figure 7.58 – 7.61. Case 12

Figure 7.62 – 7.67. Case 13

Figure 7.68 – 7.69. Case 14

Figure 7.70 – 7.72. Case 15



# **List Of Tables**

Table 1.1: Symptoms and signs of pediatric hydrocephalus.

Table 2.1: Mean values of measurements of different midsagittal distances and angles.

Table 3.1: Temporal analysis of CSF flow.

Table 3.2: Range of aqueductal peak velocities and flow in pediatric age.

Table 3.3: Range of aqueductal peak velocities and flow in normal adult age.

Table 4.1: Quantitative analysis of aqueductal CSF flow in normal control group.

Table 4.2: Descriptive statistics of aqueductal CSF parameters in the control group.

Table 4.3: Age-related variations of aqueductal CSF flow dynamics.

Table 4.4: Quantitative analysis CSF flow at upper cervical subarachnoid space in the control group.

Table 4.5: Descriptive statistics of CSF flow of the cervical subarachnoid space in the control group.

Table 4.6: Age-related variations of upper anterior cervical CSF flow dynamics.

Table 4.7: Paired samples test for comparison of CSF dynamics of the upper cervical anterior and posterior subarachnoid space.

Table 4.8: Paired samples test for comparison of temporal CSF dynamics of the aqueduct and upper cervical subarachnoid space.

Table 4.9: Clinical and conventional MRI data in patients with communicating hydrocephalus.

Table 4.10: Clinical and conventional MRI data in patients with brain atrophy.

Table 4.11: Quantitative analysis of aqueductal CSF flow in hydrocephalus group.

Table 4.12: Descriptive statistics of aqueductal CSF dynamics in the hydrocephalic patients.

Table 4.13: Quantitative analysis of aqueductal CSF flow in atrophy group.

Table 4.14: Descriptive statistics of aqueductal CSF flow parameters in atrophy patients.

Table 4.15: Comparison of aqueductal CSF dynamics among normal control, hydrocephalus and atrophy groups.

Table 4.16: Clinical and conventional MRI data in patients with aqueductal stenosis.

Table 4.17: Clinical and conventional MRI data in patients with Chiari 1 malformation and acquired tonsillar ectopia.

## **List Of Tables**

Table 4.18: Quantitative and qualitative analysis of upper cervical subarachnoid CSF flow in Chiari 1 patients and patients with acquired tonsillar ectopia.

Table 4.19: Descriptive statistics of the cervical subarachnoid CSF flow in Chiari 1 patients.

Table 4.20: Independent samples test for comparison of CSF flow parameters in the control-Chiari 1 groups.

Table 4.21: CSF flow characters inside syrinx cavities.

Table 4.22: Postoperative upper cervical CSF flow characters in Chiari 1 patients:

Table 5.1: Summary of velocity and volumetric flow values of aqueductal CSF flow reported in the literature.

## Introduction

Cardiac-cycle-related cerebral blood volume variations produce bidirectional oscillatory movement of cerebrospinal fluid (CSF) within the craniospinal axis. During systole, the net inflow of blood increases the intracranial volume and induces craniocaudal (systolic) CSF flow where the spinal subarachnoid CSF space functions as a buffer for volume expansion. During diastole, the net outflow of blood decreases the intracranial volume and promotes caudocranial (diastolic) CSF flow. A non-invasive assessment of CSF flow patterns has been found to be clinically useful where there is a disturbance of the CSF circulation (Nitz et al., 1992) (Lee et al., 2004).

Phase-contrast magnetic resonance (MR) imaging is a technique that uses a bipolar gradient pulse to impart net phase change as CSF moves along the gradient, thus sensitizing MR images to velocity changes in a specific direction, while canceling signals from stationary protons and from motion in other directions. Phase-contrast MRI is sensitive to areas of slow flow, allows flow direction to be appreciated, and permits quantification (Nitz et al., 1992) (Lee et al., 2004).

Phase-contrast MR imaging (MRI) techniques can display pulsatile CSF motion non-invasively and allows the assessment of its amplitude. Since CSF flow is pulsatile, synchronous with the cardiac cycle, cardiac gating is applied to improve temporal resolution (Nitz et al., 1992) (Bhadelia et al., 1997).

Cardiac-gated, two-dimensional (2-D) cine-phase-contrast MRI has been successfully used in evaluating patency of endoscopic third ventriculocisternostomy (Fukuhara et al., 1999), which is being increasingly used as an alternative to traditional CSF shunting in noncommunicating hydrocephalus; measuring aqueductal CSF flow in patients with normal-pressure hydrocephalus and predicting successful response to CSF shunting (Bradley et al., 1996) (Bradley, 2000); and characterizing the flow of CSF in the foramen magnum in patients with Chiari 1 malformations (Haughton et al., 2003).

## Anatomy Of The Ventricular System With MR Imaging Correlation (Crossman, 2005)

The cerebral ventricular system consists of a series of interconnecting spaces within the brain which are derived from the central lumen of the embryonic neural tube and the cerebral vesicles to which it gives rise (Fig. 1.1).

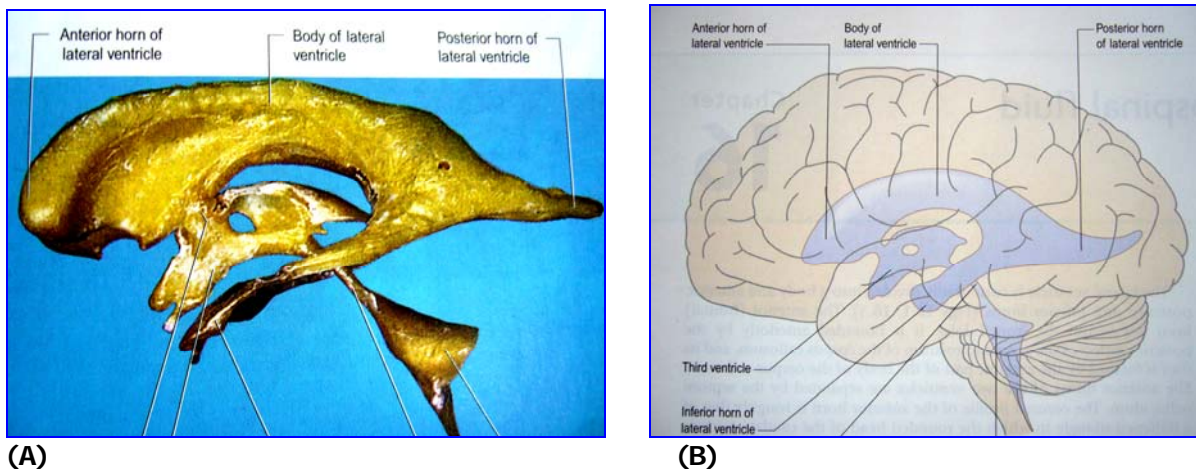
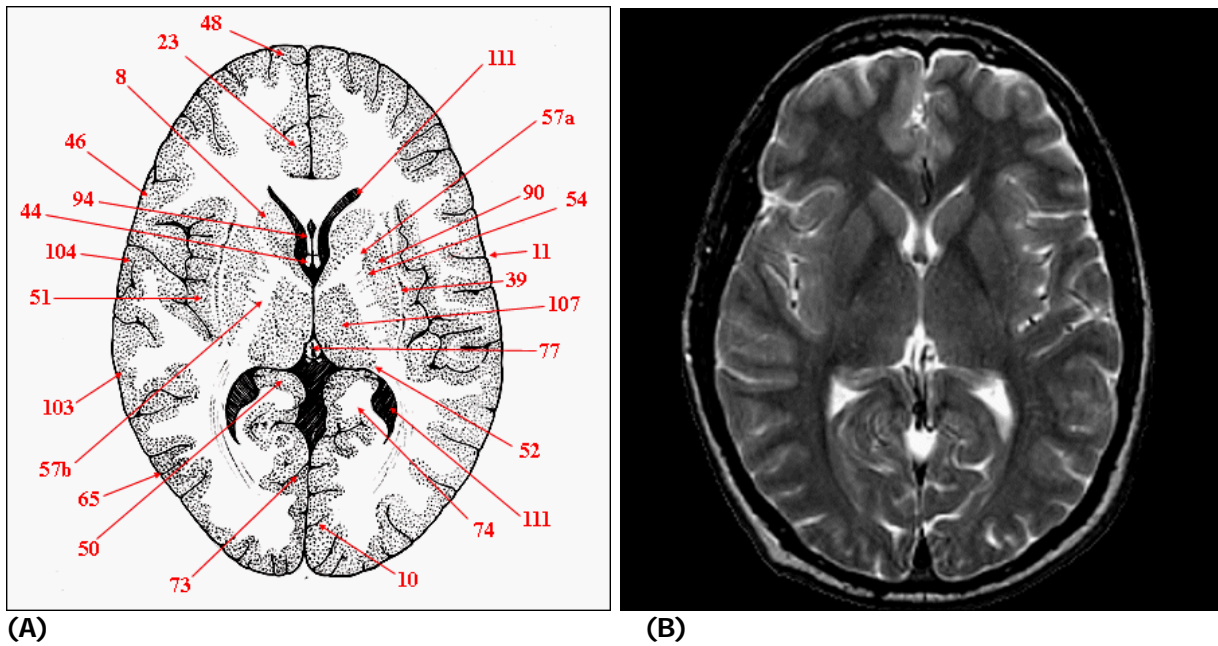


**Fig. 1.1 (Crossman, 2005): (A) Resin cast of the ventricular system. (B) Projection of the ventricular system onto the left surface of the brain.**

### Lateral Ventricle

Within the cerebral hemisphere lies the lateral ventricle. Viewed from the lateral aspect, the lateral ventricle has a roughly C-shaped profile (Fig. 1.1) with an occipital tail. It is divided into a body and frontal (anterior), occipital (posterior) and temporal (inferior) horns.

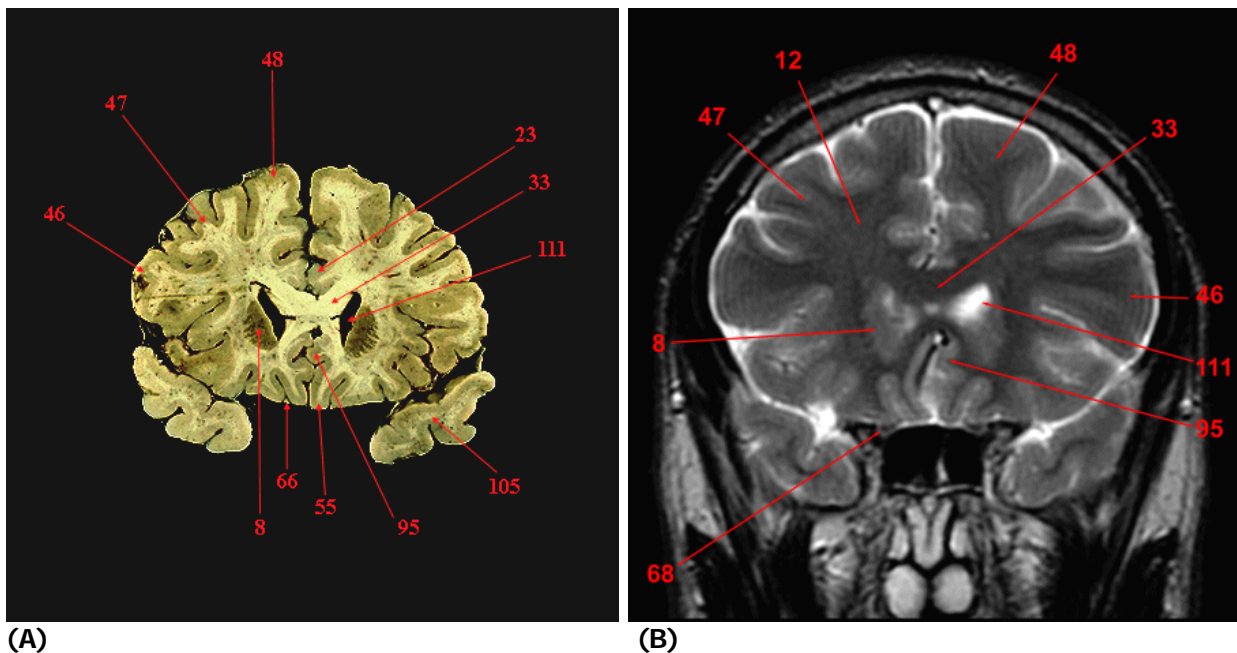
The *frontal horn* lies within the frontal lobe (Fig. 1.2 and 1.3). It is bounded anteriorly by the posterior aspect of the genu and rostrum of the corpus callosum, and its roof is formed by the anterior part of the body of the corpus callosum. The frontal horns of the two ventricles are separated by the septum pellucidum.



(A)

(B)

**Fig. 1.2 (Atlas, 2003): Diagram (A) and corresponding axial MRI image (B) of normal brain at the level of the frontal horns and atria of the lateral ventricle:**



(A)

(B)

**Fig. 1.3 (Atlas, 2003): Specimen (A) and corresponding coronal MRI image (B) of normal brain at the level of the frontal horns of the lateral ventricles**

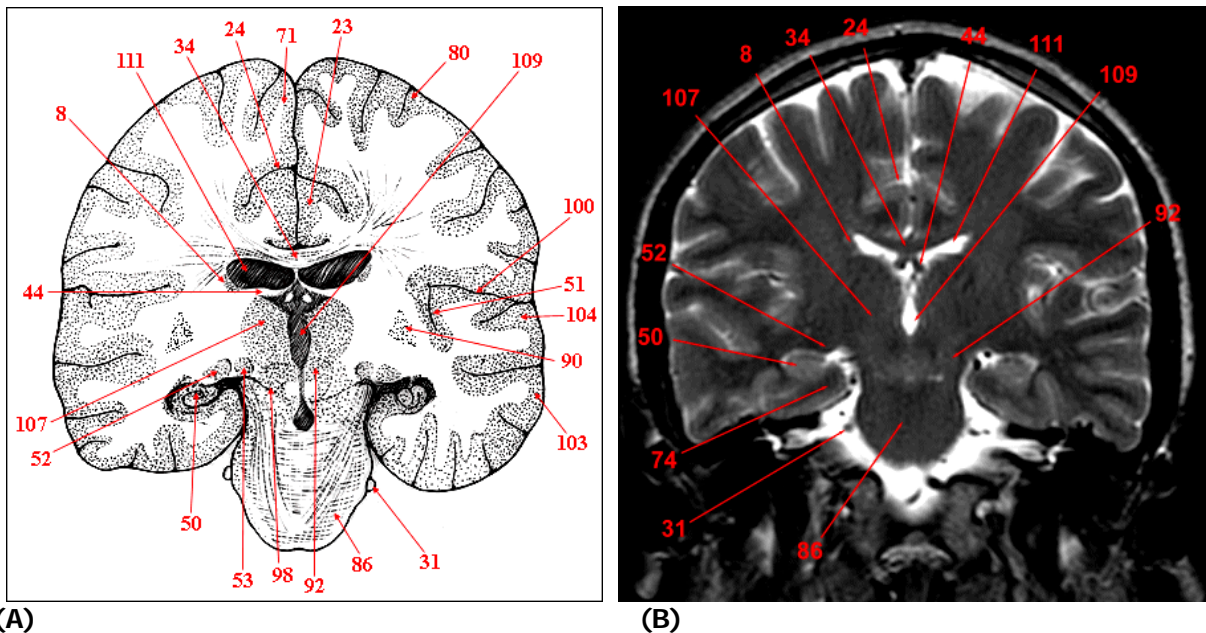
8. Caudate	51. Insular cortex	74. Parahippocampal gyrus
10. Calcarine sulcus	52. Geniculate body, lateral	77. Pineal body
11. Central sulcus	54. Globus pallidus	90. Putamen
12. centrum semiovale	55. Gyrus rectus	94. Septum pellucidum
23. Cingulate gyrus	57a. Internal capsule: anterior limb	95. subcallosal gyrus
33. Corpus callosum, genu	57b. Internal capsule: posterior limb	103. Temporal gyrus, middle
39. External capsule	65. Occipito-temporal gyri	104. Temporal gyrus, superior
44. Fornix	66. Olfactory tract and bulb	105. Temporal pole
46. Frontal gyrus, inferior	68. optic nerve	107. Thalamus
47. Frontal gyrus, middle	73. Parietal-occipital sulcus	111. Ventricle, lateral
48. Frontal gyrus, superior		
50. Hippocampus		

The coronal profile of the frontal horn (Fig. 1.3) is roughly of a flattened triangle in which the rounded head of caudate nucleus forms the lateral wall and the floor. The frontal horn extends back as far as the interventricular foramen of Monro (Fig. 1.1).

The *body* of the lateral ventricle lies within the frontal and parietal lobes, and extends from the foramen of Monro to the splenium of corpus callosum (Fig. 1.1). The bodies of the two ventricles are separated by the septum pellucidum, which contains the columns of the fornices in its lower edge (Fig. 1.4, see fig. 1.7). The inferior limit of the body and its medial wall are formed by the body of the fornix. The coronal profile of the body (Fig. 1.4) is a flattened triangle with an inward bulging lateral wall formed by the thalamus inferiorly and the tail of the caudate nucleus superiorly. The body of the lateral ventricle widens posteriorly to become continuous with the occipital and temporal horns at the *atrium* or the *trigone* of the lateral ventricle (Fig. 1.2).

The *occipital horn* curves posteromedially into the occipital lobe (Fig. 1.5). It is usually diamond-shaped or square in outline, and the two sides are often asymmetrical. Fibers of the tapetum of the corpus callosum separate the ventricle from the optic radiation, and form the roof and the lateral wall of the occipital horn. Fibers of the splenium of the corpus callosum (forceps major) pass medially as they sweep back into the occipital lobe, and produce a rounded elevation in the upper medial wall of the occipital horn.

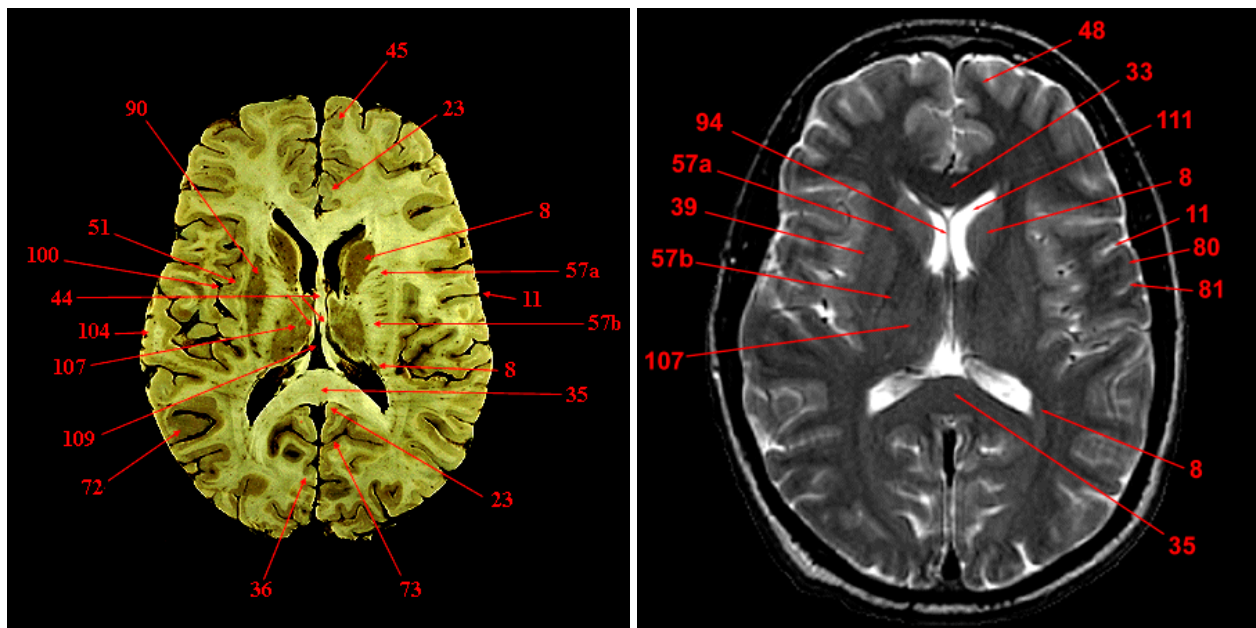




(A)

(B)

**Fig. 1.4 (Atlas, 2003): Diagram (A) and corresponding coronal MRI image (B) of normal brain at the level of the bodies of the lateral ventricles**



(A)

(B)

**Fig. 1.5 (Atlas, 2003): A specimen (A) and corresponding axial MRI image (B) of normal brain at the level of the occipital horns of the lateral ventricles**

8. Caudate	71. Paracentral lobule	102. Temporal gyrus, inferior
11. Central sulcus	72. Parietal gyri	103. Temporal gyrus, middle
23. Cingulate gyrus	74. Parahippocampal gyrus	104. Temporal gyrus, superior
24. Cingulate sulcus	80. Postcentral gyrus	107. Thalamus
31. Cranial nerve, 5th	86. Pons, base	109. Ventricle, 3rd
34. Corpus callosum, body	87. Pons, tegmentum	111. Ventricle, lateral
44. Fornix	90. Putamen	
50. Hippocampus	92. Red nucleus	
51. Insular cortex	98. Substantia nigra	
52. Geniculate body, lateral	100. Sylvian fissure	
53. Geniculate body, medial		